Modelling of Diffuse Scattering Effects for Outdoor Ray Tracing

Andrew Whelan, *Dublin City University*, Prof. Conor Brennan, *Dublin City University*

***Abstract*—Physically accurate outdoor channel modelling for high-frequency systems (e.g. 5G/6G, LiDAR, SAR) requires robust models for diffuse scattering (DS). Many established models, however, are predicated on Gaussian surface statistics.**

In this paper, we evaluate the performance of several key DS models against a numerically exact Method of Moments (MoM) solution in a 2D single-bounce scenario. By analyzing surfaces with more realistic, non-Gaussian statistics, we identify the specific regimes where these models break down, and offer guidance on the selection of the most accurate model for challenging, realistic scattering environments.

***Index Terms*—Diffuse Scattering, Diffuse Reflection, Channel Model, Ray Tracing, Ray Shooting.**

I. Introduction

THE phenomenon of diffuse scattering (DS) is understood to play a large role in outdoor scenarios, especially at high-frequencies [1]. Figure 1 illustrates the significance of high k for a simple indent.

A large class of existing models are predicated on Gaussian surface roughness (statistical models) and/or locally flat tangent planes (e.g. in asymptotic methods) . Authors in [2] identified these as weaknesses when it comes to modelling diffuse scattering for outdoor surface details. However, a broad comparison between models is lacking, especially when it comes to modelling the full $\mathbf{E}$-field.

II. Prior Work

Table I compares various models in 2d for a fixed point transmitter, a rough wall, and a line of receivers.

A. Full-Wave Models

This class of models describes computationally intensive numerical integrations of the wave equations. The model considered in this work as benchmark is the MoM model described in Algorithm 1 in Appendix A, and described in more detail in [3].

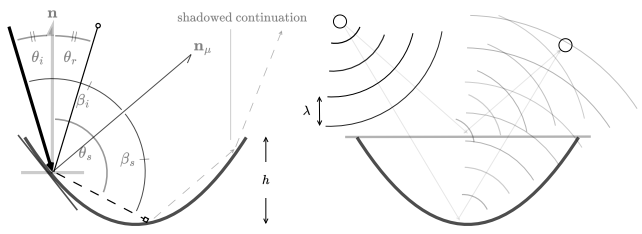

Fig. 1. A simple indent on a surface (left is the ray POV, and right is the wave POV). When indent depth (h) is comparable to, or greater than λ, as in this picture, complex interference becomes non-negligible, and the tangent plane approximation fails. This is common for the EHF-UHF range interacting with urban features.

TABLE I
Comparison of Scattering Models (see Appendix A)

Method	Class	Complexity	Limitations
MoM	Full-wave	$\mathcal{O}((k\bar{L})^3)$	- Very poor scaling - Requires big mesh
PO	Asymptotic	$\mathcal{O}((k\bar{L})^2)$	- No interscattering - Poor scaling
GO	Asymptotic	$\mathcal{O}(k\check{L}\log(k\check{L}))$	- No diffuse scattering
n-GO	Asymptotic	$\mathcal{O}(nk\check{L}\log(k\check{L}))$	- No micro-scattering

B. Asymptotic Models

In this class we find models such as the WKB hierarchy [4], PO, and GO (comprising either ray-shooting (GO-RS) or ray-tracing (GO-RT)) [3]. Since the WKB method is not widely used for ray-tracers, we only consider PO and GO.

C. Statistical Models

The prototypical model here is the Beckmann-Kirchhoff family (B-K) described in [5]. Here, the average power distribution has an analytical formula. If a further assumption is made on the phase distribution for diffuse rays, the full field can be modelled stochastically.

There are also other statistical models of note, including the Integral Equation Method [6], and the Small Slope Approximation [7], however, these won't be considered due to their computational infeasibility for ray-tracing.

D. Heuristic Models

These are a subclass of the Statistical models of section II-C where, the diffusely scattered power distribution assumes a fixed parametric form, whose parameters are empirically matched. These are further divided into models with a single parametric distribution (e.g. Phong [8], Cook-Torrance [9]), and models that use a hybrid of specular and diffuse distributions (e.g. "effective-roughness" models (ER) described in [2]).

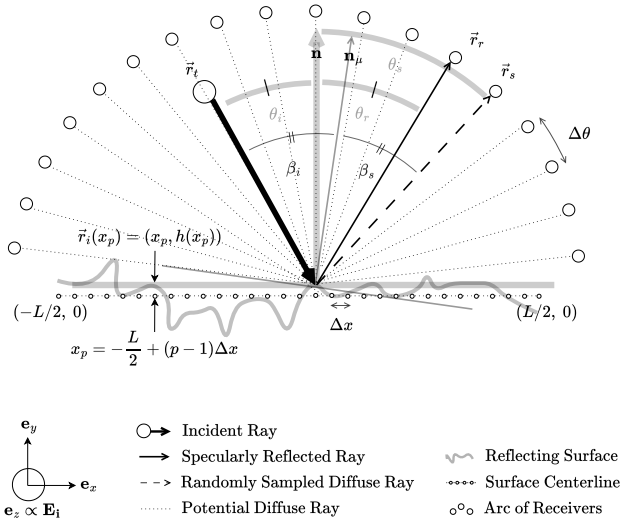

Fig. 2. Setup Geometry for ray-shooting. The surface tangents, and hence the microscopic normal ($\mathbf{n}_\mu$), β values, and scattering angle (θ_s) are assumed apropri unknown. In a stochastic model, the diffuse field $\mathbf{E}_s$ is computed for a particular ensemble according to (a) the model's PDF for θ_s, and (b) a UID phase ϕ_s.

III. Model Setup

A. Ray-Tracing vs. Ray-Shooting

In order that the models can be compared fairly, it is necessary to choose a consistent ray-propagation method. There are two broad methods:

- Ray-shooting (RS): rays are propagated from source to receiver, and
- Ray-tracing (RT): rays are propagated backward from receiver to source, using a path-length minimization algorithm.

A choice in practice is largely dependent on the receiver geometry, with the former being reserved for wide and continuous receivers. Both types are considered here, but separately.

B. Surface Modelling

The geometric setup is depicted in Figure 2. Of particular importance is modelling the surface height h. The process for Gaussian roughness is as follows, following the procedure in [10]:

1) Specify a Gaussian PDF f with RMS height deviation σ:

$$f(h) = \frac{1}{\sigma\sqrt{2\pi}} e^{-\frac{h^2}{2\sigma^2}}$$

2) Specify a surface correlation function (typically Gaussian, exponential or power-law), or equivalently the power-spectral density S. A power-law is shown here - the Hurst exponent H is a kind of fractal measure :

$$S(k) = |k|^{-(2H+1)}, \quad \text{where } H \in (0,1)$$

3) Choose a desired discretization of the target height function h, and a Nyquist determined spacing for S:

$$h[x_i], \text{ with } i \in \{0,\dots,2N-1\},\ \Delta x_i = \frac{L}{2N},$$
$$S[k_i], \text{ with } i \in \{0,\dots,N\},\ \Delta k_i = \frac{1}{L}$$

4) Sample $N-1$ UID points $\phi_1,\dots,\phi_{N-1} \in (0, 2\pi)$, and one $\phi_N \in \{0, \pi\}$ with equal probability, and set

$$z[k_i] = \begin{cases} 0, & \text{if } i = 0, \\ \sqrt{S[k_i]}e^{j\phi_i}, & \text{if } 1 \le i \le N, \\ (\sqrt{S[k_{2N-i}]}e^{j\phi_{2N-i}})^*, & \text{if } N+1 \le i \le 2N-1 \end{cases}$$

5) Perform the IFFT on z to get a surface with the correct properties (apart from RMS roughness σ):

$$h' = \text{FFT}^{-1}(z)$$

6) Rescale h' to have the correct RMS roughness:

$$\sigma' = \text{STD}(h')$$
$$h = \frac{\sigma}{\sigma'} h'.$$

Generalising this procedure to generate surfaces with a desired non-Gaussian height profile is required. Authors in [11] generalise to non-Gaussian PDFs, but here we take an efficient and reasonably realistic approach, modelling the height of a brick wall as being

1) a series of large macro structures B ('bricks') of fixed width w_B, and with random small tilts $\theta_B \sim N(\mu_{\theta_B}, \sigma_{\theta_B})$, with $0 < \mu_{\theta_B}$ small for 'lippage' effects,
2) joined by indents J ('joints') with a super-Gaussian shape (described in Figure 3), of random height ($h_J \sim N(\mu_{h_J}, \sigma_{h_J})$, and width ($w_B \sim N(\mu_{w_J}, \sigma_{w_J})$),
3) modulated by Gaussian random noise with two separate RMS roughness (σ_B, σ_J) and correlation length (ξ_B, ξ_J) parameters.

to:

1) fine manufacturing processes (subtractive),
2) coarse manufacturing processes (additive), and
3) aging defects (subtractive).

Non-Gaussian variations are due to skewness in the individual variations, and are modelled by applying a hyperbolic tangent

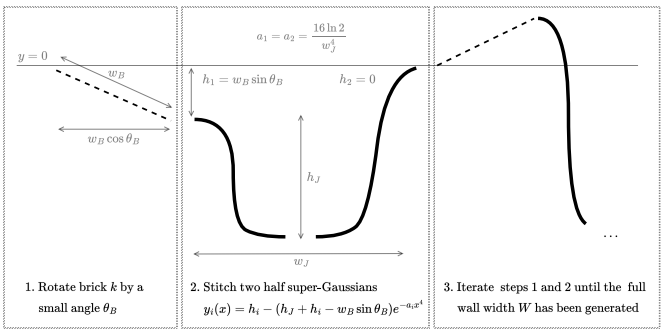

Fig. 3. Base profile for the surface height $h(x)$. The parameters a_1, a_2 are determined by setting the wall to brick joins to be at the full-width half maximum (FWHM).

to the Gaussian preprocessed functions. The result of this process is shown in Figure 4.

The height function is therefore considered as a compound of three terms:

$$h = h_{\text{coarse}} + h_{\text{fine}} + h_{\text{aging}}, \tag{1}$$

where each stage is preprocessed as a Gaussian rough surface, with postprocessing by a hyperbolic tangent and with defined RMS roughness:

- h_{coarse} is preprocessed with exponential PSD, with correlation length $l_{\text{coarse}} = 50\text{mm}$, and postprocessed with RMS roughness $\sigma_{\text{coarse}} = 5\text{mm}$,
- h_{fine} is preprocessed with Gaussian PSD, with correlation length $l_{\text{fine}} = 1\text{mm}$, and postprocessed with RMS roughness $\sigma_{\text{fine}} = 1\text{mm}$, and
- h_{aging} is preprocessed with power law PSD, with Hurst exponent $H = 0.5$, and postprocessed with RMS roughness $\sigma_{\text{aging}} = 2\text{mm}$.

C. Antenna Placement

A microcell scenario is considered. Here, the source is within a radius small enough that the curvature of the incoming wave cannot be neglected. We therefore choose a cylindrical incoming wave source at a distance 20m from the wall center, and a semi-circle of receiver antennas within a 25m distance to the wall center:

$$\vec{r}_T = \begin{bmatrix} -10\sqrt{2} \\ 10\sqrt{2} \end{bmatrix} = 20 \begin{bmatrix} -\cos\frac{\pi}{4} \\ \sin\frac{\pi}{4} \end{bmatrix} \tag{2a}$$

$$\vec{r}_R = \begin{bmatrix} -25\cos\theta_s \\ 25\sin\theta_s \end{bmatrix}, \text{ where } \theta_s \in \left(-\frac{\pi}{2}, \frac{\pi}{2}\right). \tag{2b}$$

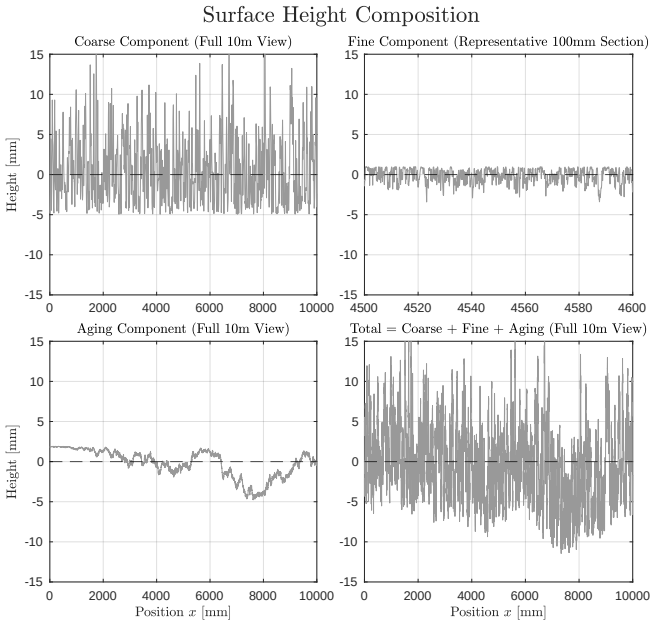

Fig. 4. $h = h_{\text{coarse}} + h_{\text{fine}} + h_{\text{aging}}$.

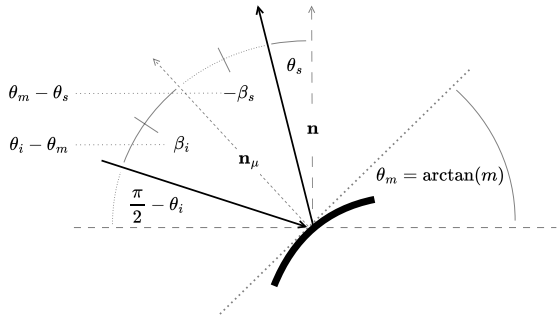

Fig. 5. μ-facet model geometry. The diagram implies that $m = \tan\left(\frac{\theta_i+\theta_s}{2}\right)$. The scattering angle PDF $f_{\Theta_s}(\theta_s)$ can be derived from this as $f_{\Theta_s}(\theta_s) = f_M(m(\theta_s))\left|\frac{dm}{d\theta_s}\right|$, where $f_M(m) = \frac{1}{\sqrt{2\pi}\sigma}e^{-\frac{m^2}{2\sigma^2}}$ is the PDF for surface slopes. The Fresnel coefficients Γ are computed with respect to $\beta_i = \frac{\theta_i-\theta_s}{2}$

D. Models Used

1) MoM Benchmark: MoM is used as a benchmark model. The basis functions used are a 1D equivalent of the Rao-Wilton-Glisson (RWG) basis functions [12], which are essentially shifted, overlapping triangular 'hats', defined on each node in the arclength domain as 1 on this node, decreasing uniformly to 0 on either side.

2) Microfacet (μ-facet): This model assumes the following (see Figure 5)

- Gaussian randomly-distributed surface-slopes,
- Locally specular ray behaviour,
- Uniformly randomly distributed reflected phase,
- Smith masking/shadowing geometric factor [13]

APPENDIX A
ALGORITHMS

For all of the below, we can obtain estimates of the numerical parameters (various N) in terms of geometrical (l_{wall}, l_{Rx}, $\bar{L}$) and wave (wavenumber k) parameters by

1) Choosing spacing $\Delta x = \frac{\lambda}{10}$ for points along the wall,
2) Choosing spacing $\Delta x = \frac{\lambda}{2}$ for points along the receiver (Nyquist criterion),
3) Converting to $\Delta x \to N, l$ by using $\Delta x = \frac{l}{N}$,
4) Converting λ to k by using $\lambda = \frac{2\pi}{k}$, and
5) (Optionally) use the GM length $\bar{L} \overset{\text{def}}{=} \sqrt[N_l]{(\prod_{i=1}^{N_l} l_i)}$, or in the case of log factors, use the maximum dimension $\check{L} \overset{\text{def}}{=} \max_{i=1}^{N_l} l_i$

Algorithm 1: Method of Moments (MoM)

$$\mathcal{O}((k \cdot \bar{L})^3) = \mathcal{O}\left(\left(\tfrac{5}{\pi}\right)^3 \cdot k^3 \cdot l_{\text{wall}}^3\right) = \mathcal{O}(N_b^3) = \mathcal{O}(N_b^2 + N_b^3 + N_b \cdot N_R)$$

for $m \leftarrow 1$ **to** N_b **do**
  $\mathbf{V}_m \leftarrow \langle \mathbf{E}_i(\vec{r}_T), g_m \rangle$;
  for $n \leftarrow 1$ **to** N_b **do**
    $\mathbf{Z}_{mn} \leftarrow \langle \mathcal{L}(f_n), g_m \rangle$;
  end
end
Solve $\mathbf{Za} = \mathbf{V}$ for the unknown current coefficients $\mathbf{a}$;
for N_R *points* $\vec{r}_R$ *on receiver* **do**
  $\mathbf{E}_R(\vec{r}_R) \leftarrow 0$;
  for $n \leftarrow 1$ **to** N_b **do**
    $\mathbf{E}_R(\vec{r}_R) \leftarrow \mathbf{E}_R(\vec{r}_R) + \mathbf{a}_n \cdot \mathcal{L}(f_n)(\vec{r}_R)$;
  end
end
return $\mathbf{a}, \mathbf{E}_R$

Algorithm 2: Physical Optics (PO)

$$\mathcal{O}((k \cdot \bar{L})^2) = \mathcal{O}\left(\tfrac{5}{\pi^2} \cdot k^2 \cdot l_{\text{wall}} \cdot l_{\text{Rx}}\right) = \mathcal{O}(N_S \cdot N_R) = \mathcal{O}(N_S + N_S \cdot N_R)$$

for N_S *points* $\vec{r}_S$ *on the wall* **do**
  $\hat{n}(\vec{r}_S) \leftarrow \text{normal}(\vec{r}_S)$;
  $\mathbf{E}_S(\vec{r}_S) \leftarrow \sqrt{\frac{P_T \eta k}{2}} \mathcal{G}(k \|\vec{r}_S - \vec{r}_T\|) \hat{\mathbf{k}}$;
  $\mathbf{H}_S(\vec{r}_S) \leftarrow -\frac{j}{\eta k} \nabla \times \mathbf{E}_S$;
  $J_S(\vec{r}_S) \leftarrow 2\hat{n} \times \mathbf{H}_S$;
end
for N_R *points* $\vec{r}_R$ *on receiver* **do**
  $\mathbf{E}_R(\vec{r}_R) \leftarrow 0$;
  for N_S *points* $\vec{r}_S$ *on the wall* **do**
    $\mathbf{E}_R(\vec{r}_R) \leftarrow \mathbf{E}_R(\vec{r}_R) + \Delta_S \mathcal{G}(k \|\vec{r}_R - \vec{r}_S\|) J_S(\vec{r}_S)$;
  end
  $\mathbf{E}_R(\vec{r}_R) \leftarrow -\frac{k\eta}{4} \mathbf{E}_R$;
end
return $\mathbf{E}_R$

Algorithm 3: Geo. Optics – Ray Shooting (GO-RS)

$$\mathcal{O}(N_{\text{rays}} \cdot \log(N_S))$$

for $n \leftarrow 1$ **to** N_{rays} **do**
  Generate initial ray $(\hat{\mathbf{k}}_i, E_0)$ from source $\vec{r}_T$;
  $\vec{r}_S \leftarrow \text{find\_intersection}(\hat{\mathbf{k}}_i, \vec{r}_T, \text{mesh}_S)$;
  if *no intersection* **then**
    continue;
  end
  $\hat{n} \leftarrow \text{get\_normal}(\vec{r}_S)$;
  if *ray hits from behind* **then**
    continue;
  end
  $\hat{\mathbf{k}}_r \leftarrow \text{reflect}(\hat{\mathbf{k}}_i, \hat{n})$;
  $\vec{r}_R \leftarrow \text{find\_intersection}(\hat{\mathbf{k}}_r, \vec{r}_S, \text{mesh}_R)$;
  if *no intersection* **then**
    continue;
  end
  $\Gamma \leftarrow \text{fresnel\_coefficient}(\hat{\mathbf{k}}_i, \hat{n})$;
  $\mathcal{D} \leftarrow \text{divergence}(\vec{r}_T, \vec{r}_S, \vec{r}_R, \text{curvatures})$;
  $\text{pathLen} \leftarrow \|\vec{r}_S - \vec{r}_T\| + \|\vec{r}_R - \vec{r}_S\|$;
  $\mathbf{E}_R(\vec{r}_R) \leftarrow \mathbf{E}_R(\vec{r}_R) + E_0 \cdot \Gamma \cdot \mathcal{D} \cdot e^{jk \cdot \text{pathLen}}$;
end
return $\mathbf{E}_R$

Algorithm 4: Beckmann-Kirchhoff (B-K)

$$\mathcal{O}() = \mathcal{O}() = \mathcal{O}() = \mathcal{O}()$$

for $n \leftarrow 1$ **to** N **do**
  $(\text{path\_found}, \vec{r}_T, \vec{r}_S, \vec{r}_R, \text{weight}) \leftarrow \text{generate\_path}(\text{method})$;
  if *not path_found* **then**
    continue;
  end
  $\theta_i \leftarrow \text{calc\_angle}(\vec{r}_T, \vec{r}_S, \text{normal}(\vec{r}_S))$;
  $\theta_s \leftarrow \text{calc\_angle}(\vec{r}_R, \vec{r}_S, \text{normal}(\vec{r}_S))$;
  $\Gamma \leftarrow \text{fresnel\_coefficient}(\theta_i, \eta_r)$;
  $F \leftarrow \text{scattering\_factor}(\theta_i, \theta_s, \Gamma)$;
  $\text{pathLen} \leftarrow \|\vec{r}_S - \vec{r}_T\| + \|\vec{r}_R - \vec{r}_S\|$;
  $E_{path} \leftarrow \frac{E_0}{\text{pathLen}} \cdot F \cdot e^{jk \cdot \text{pathLen}}$;
  $E_{final\_contrib} \leftarrow E_{path} \cdot \text{weight}$;
  $E_{diff}(\vec{r}_R) \leftarrow E_{diff}(\vec{r}_R) + E_{final\_contrib}$;
end
for *each* R *in* R_{set} **do**
  $E_{diff}(R) \leftarrow \frac{1}{N} E_{diff}(R)$;
end
return E_{diff}

REFERENCES

[1] V. Degli-Esposti "A diffuse scattering model for urban propagation prediction", IEEE Transactions on Antennas and Propagation, vol. 49, no. 7, pp. 1111-1113, July 2001.

[2] E. M. Vitucci, N. Cenni, F. Fuschini and V. Degli-Esposti, "A Reciprocal Heuristic Model for Diffuse Scattering From Walls and Surfaces", IEEE Transactions on Antennas and Propagation, vol. 71, no. 7, pp. 6072-6083, July 2023.

[3] C. A. Balanis, "Advanced Engineering Electromagnetics", 2nd ed. Hoboken, NJ: John Wiley & Sons, Inc., 2012.

[4] C. M. Bender and S. A. Orszag, "Advanced Mathematical Methods for Scientists and Engineers I: Asymptotic Methods and Perturbation Theory". New York: Springer-Verlag, 1999.

[5] Hossein Ragheb, Edwin R. Hancock, "The modified Beckmann–Kirchhoff scattering theory for rough surface analysis", Pattern Recognition, Volume 40, Issue 7, 2007, Pages 2004-2020, ISSN 0031-3203.

[6] A. K. Fung, Z. Li, and K. S. Chen, "Backscattering from a randomly rough dielectric surface," *IEEE Trans. Geosci. Remote Sens.*, vol. 30, no. 2, pp. 356–369, Mar. 1992.

[7] A. G. Voronovich, "Wave Scattering from Rough Surfaces", 2nd ed. Berlin, Heidelberg: Springer-Verlag, 1999.

[8] B. T. Phong, "Illumination for computer generated pictures," *Commun. ACM*, vol. 18, no. 6, pp. 311–317, Jun. 1975.

[9] R. L. Cook and K. E. Torrance, "A reflectance model for computer graphics," *ACM Trans. Graph.*, vol. 1, no. 1, pp. 7–24, Jan. 1982.

[10] J. J. Wu, "Simulation of rough surfaces with FFT", Tribology International **33**, 47 (2000).

[11] T. Schreiber and A. Schmitz, *Surrogate time series*, Physica D: Nonlinear Phenomena **142**, 346 (2000).

[12] S. M. Rao, D. R. Wilton, and A. W. Glisson, "Electromagnetic scattering

by surfaces of arbitrary shape", *IEEE Transactions on Antennas and Propagation*, vol. 30, no. 3, pp. 409-418, May 1982.

[13] X. D. He, K. E. Torrance, F. X. Sillion, and D. P. Greenberg. "A comprehensive physical model for light reflection.", *Computer Graphics (Proceedings of SIGGRAPH '91)*, vol. 25, pages 175–186, July 1991